Stability of point defects near MgO grain boundaries in FeCoB/MgO/FeCoB magnetic tunnel junctions

Jonathan J. Bean[1,*] and Keith P. McKenna[2,†]

[1]*Department of Materials Science and Metallurgy, The University of Cambridge, Cambridge, CB3 0FS, UK*

[2]*Department of Physics, The University of York, York, YO10 5DD, UK*

(Dated: November 28, 2018)

Abstract

Magnetic tunnel junctions employing FeCoB as the ferromagnet and MgO as a spacer layer exhibit high performance and are attractive for magnetic random access memory applications. On post-deposition annealing B is observed to diffuse out of the FeCoB layers inducing crystallization of FeCo. It is known that a large proportion of B escapes into the adjacent tantalum underlayer. While diffusion of B into bulk MgO is known to be unfavorable it is possible that B could diffuse into grain boundaries (GBs) in the polycrystalline MgO layer, affecting its electronic properties. In this paper density functional theory is used to investigate the stability and electronic properties of oxygen vacancy and B interstitial defects at MgO GBs. We show that both types of defects exhibit increased stability at the GBs and introduce electronic states in the gap that could negatively impact performance. These predictions are consistent with recent experimental results and we discuss further means to confirm the results experimentally using techniques such as x-ray or ultra-violet photoelectron spectroscopy.

I. INTRODUCTION

Magnetic tunnel junctions (MTJs) are a key functional component in magnetic random access memory (MRAM) which offer significant benefits over traditional DRAM technology,[1–3] including non-volatility and high read/write speeds. MTJs are already used in hard disk read heads and there is scope for their use in other components such as high density L1\L2\L3 cache memory[4,5]. MTJs contain an insulating non-magnetic spacer layer which is sandwiched between two ferromagnetic layers[6,7]. The resistance of an MTJ depends on the relative alignment of the magnetisation in the two ferromagnetic electrodes (i.e. parallel or anti-parallel). The ratio between the difference in resistance between the parallel and anti-parallel configurations is known as the tunneling magnetoresistance (TMR). The devices which exhibit the largest TMR use FeCoB as the electrode material and MgO as the insulating barrier[8]. Bloch states with different symmetries decay with different rates through the MgO barrier leading to a strong spin filtering effect in MgO and large TMR[9].

There is a discrepancy between the theoretically predicted TMR ($\sim$2000 %) and the experimentally observed TMR for MgO based MTJs (up to 604 %)[8,10–14]. One explanation is that defects such as grain boundaries (GBs) and point defects, which are not usually included in theoretical models, could be affecting the electronic properties of the MgO barrier. Past work by the authors showed the types and presence of GBs in the MgO layer and their potential impact on the TMR via scanning transmission electron microscopy (STEM) images and first principles calculations[15]. However, a theoretical investigation of point defects located at the experimentally observed GBs in MgO MTJs is so far missing.

There are two types of point defects considered in this paper that could influence electronic transport in MTJs and negatively impact the TMR. The first are oxygen vacancies which could be stabalized at MgO GBs due to the decreased coordination and the smaller binding energy of oxygen atoms in the MgO lattice. Experimental evidence such as photoemmission spectroscopy has shown that oxidation of the Fe electrode can occur near the MgO layer in MTJs[16] suggesting transport of oxygen from the bulk MgO towards the Fe layer. Electron probe micro-analysis has been unable to detect oxygen vacancies within MgO which suggests that they are not present in significant quantities, but small concentrations of oxygen vacancies could influence the TMR[13]. Theoretical calculations using density functional theory (DFT) have shown that oxygen vacancies are energetically more stable at GBs than in the bulk[17–19].

The second type of point defect we consider are boron interstitials. MTJs are usually annealed to crystallise the FeCoB which is usually amorphous on deposition. The annealing process increases the TMR as amorphous metals have a lower conductivity and smaller TMR due to the reduced spin filtering effect. Following annealing boron escapes from the FeCoB layer into another layer in the MTJ stack[20]. However experimental studies are not in agreement on the mechanism of transport of B after annealing within the FeCoB electrode with some studies reporting that boron diffuses into the tantalum[20] and others reporting that the boron can escape into the MgO[21,22]. If boron is found in the MgO layer it has been shown to exist in the B^{3+} charge state[23]. Theoretical calculations show that B in bulk MgO is not stable with respect to the FeCoB electrode[20]. In addition DFT calculations have also been performed on the Fe/MgO interface showing that certain boron interstitial locations are energetically stable[24]. DFT calculations have shown that B can exist in an energetically stable form at the surfaces of MgO[25]. Theoretical calculations have also shown that the addition of B within MgO can give rise to magnetic moment of the B in MgO[26].

In this paper first principles calculations are performed to investigate the structural stability of oxygen vacancies and boron interstitials near GBs in MgO. It is found that there is a strong preference for oxygen vacancies and boron interstitials to segregate to the GBs. For the stable boron interstitials the electronic properties have been calculated using a hybrid functional (HSE06) to allow for better comparison between theory and experiment[27]. Using techniques such as x-ray photoelectron spectroscopy (XPS) or ultra-violet photoelectron-spectroscopy (UPS) predictions made in this paper could be verified.

The rest of this paper is structured in the following way. In Sec. II we describe the computational methods employed to construct the GB models and how point defects within these models are created. In Sec. III we discuss the results for the oxygen vacancies and boron interstitials. In Sec. IV the results are discussed and in Sec. V the main findings of the research is summarised.

II. METHODS

Point defects in MgO are investigated using bicrystal supercells. The supercells were constructed based on structural unit geometries found in STEM images previously reported[15]. There are two GBs which are considered: $\Sigma5(210)[001]$ symmetric tilt grain boundary (STGB) and (100)/(110)[001] asymmetric tilt grain boundary (ATGB). The former contains 152 atoms and the latter 266 atoms. The stable structures for both GBs are obtained using the γ-surface method, i.e.

optimization of the total energy with respect to the position of all atoms and translation of one grain relative to the other[19,28,29]. For point defect calculations the GB the supercells are expanded in the [001] direction to minimise unphysical interactions between periodic images. Here the cells were expanded to four layers (from two layers) resulting in a minimum distance of 8.52 Å between periodic images to give the balance between reasonable results and computational feasibility. This results in a 304 atom supercell for the STGB and 532 atom supercell for the ATGB shown in Fig. 1. We find the same relative ordering of defect segregation energies for both the STGB and ATGB using both the two-layer and four-layer supercells. We also verified that use of a larger six-layer supercell does not significantly change segregation energies (see Results section below).

The stability of any defect can be determined by computing the formation energy,

$$E_{\mathrm{f}} = E^{q}_{\mathrm{ideal}} - E_{\mathrm{def}} + \sum_{i} \mu \Delta N + q \Delta E_{\mathrm{F}}, \tag{1}$$

where E^{q}_{ideal} is the energy of the ideal system, E_{def} is the energy of the defective system, μ is the chemical potential corresponding to the species added or removed, ΔN is the difference in the number of atoms between the ideal and defective systems, q is the difference in the charge and E_{F} is the Fermi energy. The total energy of a defect in the centre of a grain can be selected as a reference to calculate the segregation energy E_{seg}.

We compute the segregation energy for oxygen vacancies and boron interstitials within 10 Å of the GB (considering only defects inequivalent by symmetry). A total of 16 oxygen vacancy sites in the Σ5(210)[001] STGB and 75 vacancy sites in the (100)/(110)[001] ATGB were considered. For the MgO STGB there were two different structural configurations found which are stable. However experimentally using STEM only one structure was detected, it is this structure which is higher in energy which is considered for study in this paper[15]. When studying the oxygen vacancies in the MgO STGB system the energy tolerance had to be higher (0.03 eV/Å rather than 0.01 eV/Å) to ensure that the system did not revert to the lower energy open structure. This reversion is likely to be an unphysical effect associated with the small grain sizes of the supercells selected, but the tolerance is small enough to ensure that the results are otherwise reliable. To generate the boron interstitials a 3D grid which overlays the supercell is defined. Boron interstitials were inserted at points in the grid ensuring that no boron atom inserted is too close to another atom. A total of 24 prospective boron interstitial sites were identified in the Σ5(210)[001] STGB and 51 sites in the (100)/(110)[001] ATGB. A full relaxation of atomic positions of the atoms is performed on the GB supercells to determine the segregation energy for both oxygen vacancies and boron interstitials.

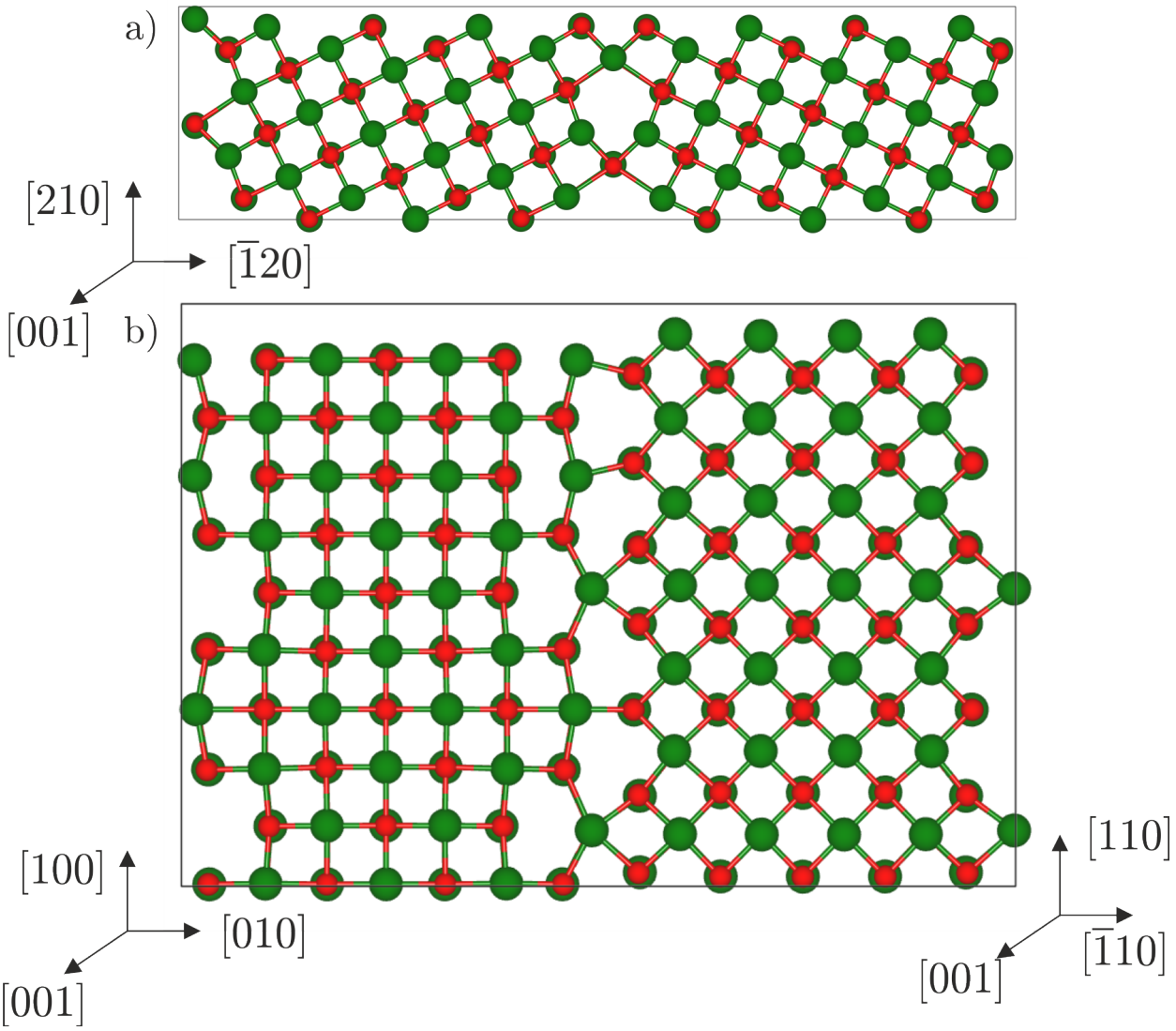

FIG. 1. Theoretical models of stable MgO grain boundary supercells. a) Σ5(210)[001] symmetric tilt grain boundary. b) (100)/(110)[001] asymmetric tilt grain boundary. Red and green atoms represent O and Mg respectively.

We perform first principles calculations within the formalism of density functional theory (DFT)[30,31]. Calculations are carried out using the Vienna Ab-initio Simulation Package (VASP)[32,33]. The generalized gradient approximation (GGA) with the parameterization of Perdew, Burke and Ernzerhof (PBE) has been used to describe the exchange correlation energy[34]. To determine the defect segregation energies the wavefunctions are expanded in a plane-wave basis with energies up to 350 eV and a Monkhorst-Pack *k*-point mesh grid centred at the gamma point of $1\times6\times3$ for the STGB supercells and $1\times6\times1$ for the ATGB supercells. All atoms in the supercells were fully

optimised with respect to interatomic force tolerance of 0.01 eV/Å. Single point calculations were performed on optimised structures using the hybrid HSE06 functional to determine the electronic density of states (DOS). The supercells were rescaled according to the bulk MgO optimised lattice constants obtained using the HSE06 functional to minimise strain, then electronically converged.

III. RESULTS

Properties of pristine grain boundaries

To provide insight into the electronic properties of the pristine GBs we first compute the on-site electrostatic potential using PBE functionals for all sites in both GB models (shown in Fig. 2). The on-site electrostatic potential is calculated by integrating the potential with a unit test charge (radius 0.87 Å for O and 0.83 Å for Mg). For O sites in the Σ5(210)[001] STGB there are variations in the on-site electrostatic potential within ± 5 Å of the GB plane. However, for the O site at the GB plane the electrostatic potential is similar to that in the bulk. In the case of Mg in the STGB there is a similar variation in potential near the GB however the Mg site at the GB has a slightly lower electrostatic potential than in the bulk. For both O and Mg sites (100)/(110)[001] ATGB there is again a region within ± 5 Å of the GB plane in which the on-site electrostatic potential varies considerably. The difference between the highest and lowest electrostatic potential is at a maximum at the GB plane indicating considerable site-to-site variations at the ATGB. One would expect these variations be reflected in variations in the position of gap states associated with point defects. Indeed, this is what we find for oxygen vacancies (discussed in the following section). We note that the difference between the electrostatic potentials calculated using PBE and HSE functionals is a constant shift of 7 eV for Mg sites and 6 eV for O sites and does not change the form of the variation near the grain boundaries.

Oxygen vacancies

The variation of segregation energy with respect to position of oxygen vacancies in the Σ5(210)[001] STGB and (100)/(110)[001] ATGB is shown in Fig. 3a & b. Due to symmetry it is only necessary to compute properties for oxygen vacancies on one side of the interface for the MgO Σ5(210)[001] STGB but results have been mirrored about the GB plane. It is observed that

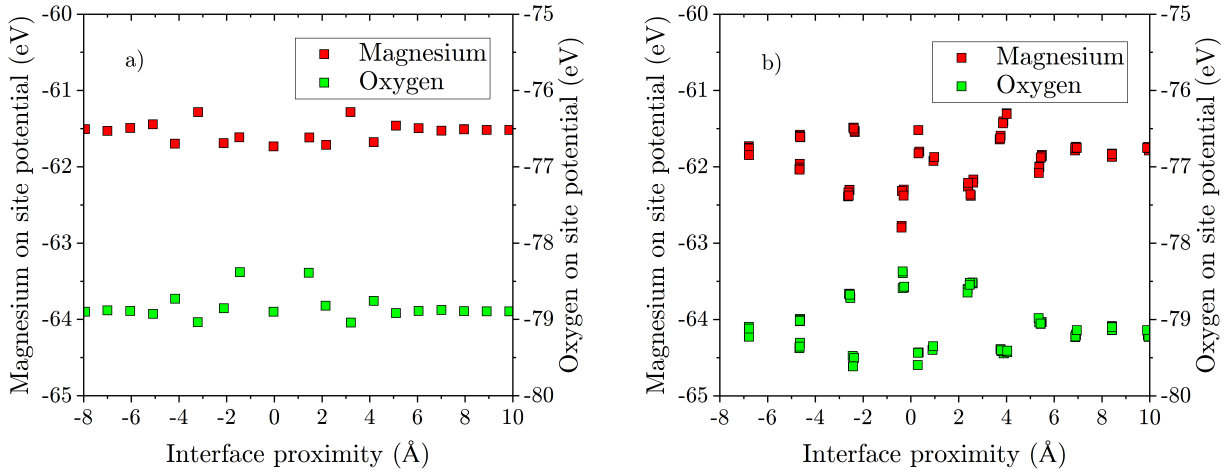

FIG. 2. On-site electrostatic potential (obtained using the PBE functional) for point defect free theoretical models of the grain boundaries. a) MgO Σ5(210)[001] symmetric tilt grain boundary b) MgO (100)/(110)[001] asymmetric tilt grain boundary.

the neutral oxygen vacancies (in Kröger-Vink notation $V_O^{\times}$) are around 0.5 eV more stable than the bulk at the Σ5(210)[001] STGB and 1.8 eV more stable than the bulk at the (100)/(110)[001] ATGB. The higher segregation energy at the GBs is due to the decreased coordination of the atoms at the interface. The lower coordination means that the atoms are less tightly bound and thus it is easier for atoms to be removed. We also performed additional calculations for a 6-layer cell finding segregation energies for the most stable O vacancy defect in the ATGB of 2.6 eV (2 layers), 1.8 eV (4 layers) and 1.96 eV (6 layers). The difference in segregation energy between the 6- and 4-layer system is < 0.2 eV and so is sufficiently converged to give confidence in the results. High segregation energies at the GBs suggest that there may be a higher concentration of oxygen vacancies in this structure than in the bulk material. The higher segregation energy of the (100)/(110)[001] ATGB suggests that oxygen vacancies are extremely likely to occur at boundaries of this type. It is difficult to characterize structural relaxation at the GBs as there are other processes such as general GB relaxation which can modify the structure. In the bulk however the level of structural relaxation around oxygen vacancies in both Σ5(210)[001] STGB and the (100)/(110)[001] ATGB is low (usually less than 2% strain).

To highlight how the electronic properties change with the addition of oxygen vacancies the projected density of states (PDOS) for the most stable oxygen vacancies and pristine GBs are shown in Fig. 4. It is observed that the oxygen vacancies create an unoccupied state in the centre

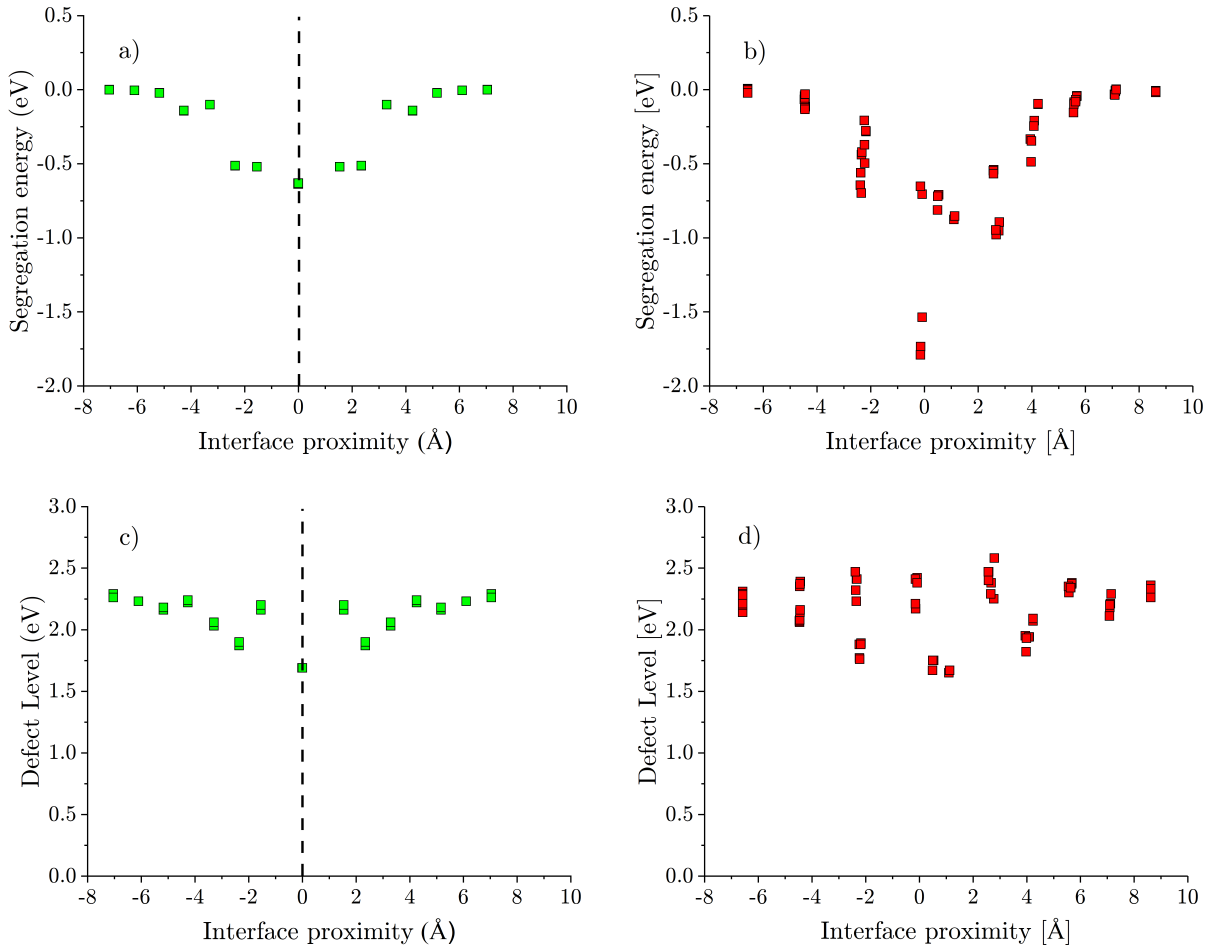

FIG. 3. Relationship between segregation energy and location of oxygen vacancies in relation to proximity to the grain boundary, and differences in energy between valence band maximum and oxygen vacancy defect level for oxygen vacancies in grain boundary models. a) Σ5(210)[001] symmetric tilt grain boundary oxygen vacancy segregation energy, b) (100)/(110)[001] asymmetric tilt grain boundary oxygen vacancy segregation energy, c) MgO symmetric tilt grain boundary oxygen defect level and d) MgO asymmetric tilt grain boundary oxygen defect level.

of the gap. The location of the oxygen vacancy defect level for both the STGB and ATGB is similar in energy but is located in different positions relative to the conduction band. The band gap is also much smaller in the ATGB over the STGB as previously reported[15]. See Supplemental Material at [URL will be inserted by publisher] for structures of the oxygen vacancies in the STGB and ATGB (Figs.S1 & S2)[35].

To further examine the effect of the location of oxygen vacancies the difference in energy

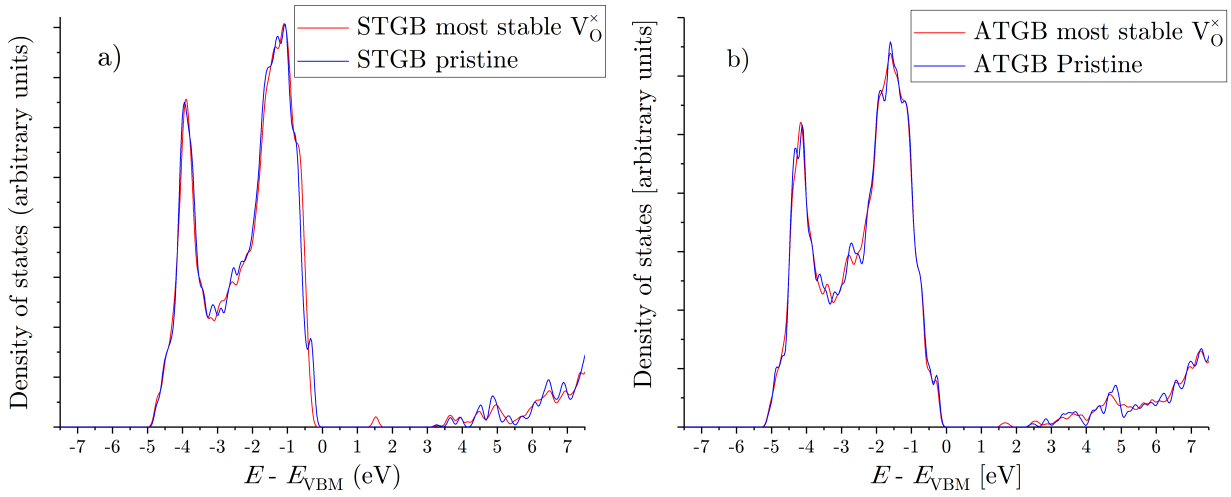

FIG. 4. Density of states computed at the PBE level for most stable oxygen vacancies and pristine grain boundary systems in a) MgO Σ5(210)[001] symmetric tilt grain boundary and b) MgO (100)/(110)[001] asymmetric tilt grain boundary.

between the valence band maximum (E_{VBM}) and the oxygen vacancy defect level in the gap has been determined for each oxygen vacancy using the PBE functional (shown in Fig. 3c & d). The reference point for E_{VBM} is taken from the bulk in each system. In the case of the Σ5(210)[001] STGB there is a slow reduction of the defect level position from a position which is already bulk like (-6 Å) with the most stable oxygen vacancy at the GB having the deepest defect level position. In the case of the (100)/(110)[001] ATGB there is both an increase and decrease in the defect level position with proximity to the GB. The presence of oxygen vacancies and shifts of the oxygen defect level in the gap in MgO is likely to adversely affect electronic transport. The defect level position is more sensitive to strain than the segregation energy with additional states being present near the top of the valence band in the ATGB (See Supplemental Material at [URL will be inserted by publisher] in Figs.S5 & S6[35]).

Boron interstitials

The incorporation of B into a neutral oxygen vacancy ($B_O^\times$) has a formation energy of only 4.2 eV in the bulk. However, if boron point defects were introduced into oxygen vacancy sites in either the STGB or ATGB the structure was found to significantly deform and give a much higher energy state thus no further analysis of these types of defect is needed. Next we discuss the results

for boron interstitials. We consider boron interstitials in the $B_i^{\bullet\bullet\bullet}$ charge state as this is found to be most stable in bulk[20]. The segregation energy of the boron interstitial can be calculated in the same way as the oxygen vacancies (see Eqn. 1). This defect is implicitly charge compensated by a uniformly distributed jellium background (equivalent to setting the average electrostatic potential to zero). We do not include higher order charge corrections since we expect these to be very similar in magnitude for the different sites. Therefore, segregation energies (which are differences in the formation energy for two different sites) should not be affected.

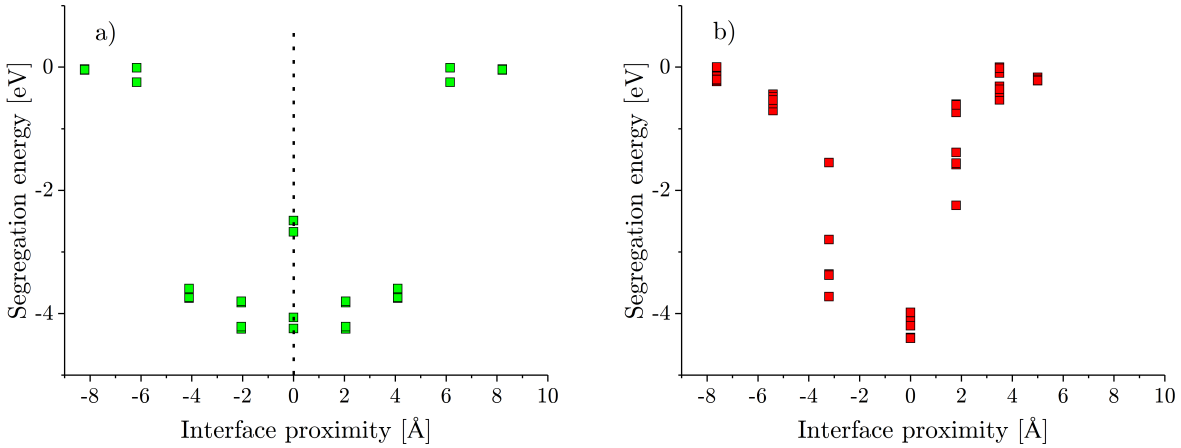

FIG. 5. Relationship between segregation energy of a single boron interstitial as a function of the interface proximity. a) MgO Σ5(210)[001] symmetric tilt grain boundary b) MgO (100)/(110) asymmetric tilt grain boundary.

In Fig. 5 the segregation energy for the boron interstitials near a Σ5(210)[001] STGB and a (100)/(110)[001] ATGB is shown. It is observed that there is a maximum segregation energy of approximately 4 eV in both GBs. We find the main difference between the 2 and 4 layer supercells is an approximately uniform reduction in the segregation energies obtained of around 30% which does not affect the general trend. In the case of the Σ5(210)[001] STGB the stable boron interstitials at the GB significantly perturb the geometry of the GB, exist in the 3+ charge state and are bonded directly with three oxygen atoms (See Supplementary Material at [URL will be inserted by publisher] Figs.S3 & S4 for structures[35]). In the bulk the B is bonded in the tetrahedral orientation to four oxygen atoms and adopts the $B_i^{\bullet\bullet\bullet}$ configuration. There is some structural relaxation of the oxygen and magnesium atoms in bulk around the boron interstitial in bulk. The stable boron interstitials are all located inside the large voids in the ATGB (Fig. 6a).

The segregation energy gives an indication of where boron interstitials could be located in the MgO GBs but it is difficult to compare directly to experiments. To aid comparison to experiment the theoretical PDOS is computed for two systems of interest (the pristine MgO ATGB and a boron interstitial in the most stable position at the ATGB). The PDOS provides insight into the effect that B point defects have on the electronic properties of the MgO as well as providing a link to spectroscopic properties that are accessible experimentally. The presence of boron in the positive charge state creates additional states which are lower than bulk MgO and so may be detectable experimentally albeit indirectly. The calculated PDOS are shown in Fig. 6b. In the case of the boron interstitial near the GB it is observed that there are two additional peaks which appear below the valence band which are not present in bulk MgO ATGB or STGB[15]. The presence of $B_i^{\bullet\bullet\bullet}$ induces localized states which are lower than those far away from the defect. The boron interstitials at the GBs also create additional unoccupied defect states in the band gap around 3 eV above the valence band maximum. Therefore, in the presence of an electrode with a valence band offset around 3 eV or larger one could expect the 2+ B interstitial to become thermodynamically favorable at the GB. Indeed we find that an electron added to the supercell containing a boron interstitial in the most stable position at the ATGB localizes on the B ion forming $B_i^{\bullet\bullet}$. Importantly, the band gap in the presence of B is 1 eV smaller than in the case of the pristine ATGB.

Previous DFT calculations have shown that is is possible for B to become slightly magnetised in Fe/MgO interfaces[26]. In our calculations there is a small magnetic moment (~ 0.01) on B, it could be that the presence of Fe near boron as in the FeCoB/MgO/FeCoB interfaces induces additional magnetic moment of boron. The effect of additional magnetic polarisation on the segregation energy is small and does not significantly change any conclusions in this paper.

To allow for easy comparison to experiment the photoelectron spectra has been simulated using a code developed by the group of Prof. David Scanlon called GALORE[36]. GALORE extracts and interpolates the cross sectional weights from reference data and generates tabulated data for experimental comparison. The probability of photoionisation is based on radiation, orbital energies and their shape. To account for this weighting must be applied according to their photoionisation cross-sections. GALORE uses the Gelius method to perform the weighting[37]. In Fig. 6c we show the simulated XPS spectrum for a the boron interstitial at the GB and no boron interstitial. The simulated XPS data could be used to validate the prediction that if $B_i^{\bullet\bullet\bullet}$ is located at the GBs as there will be the appearance of two additional peaks in the measured XPS spectrum before the valence band.

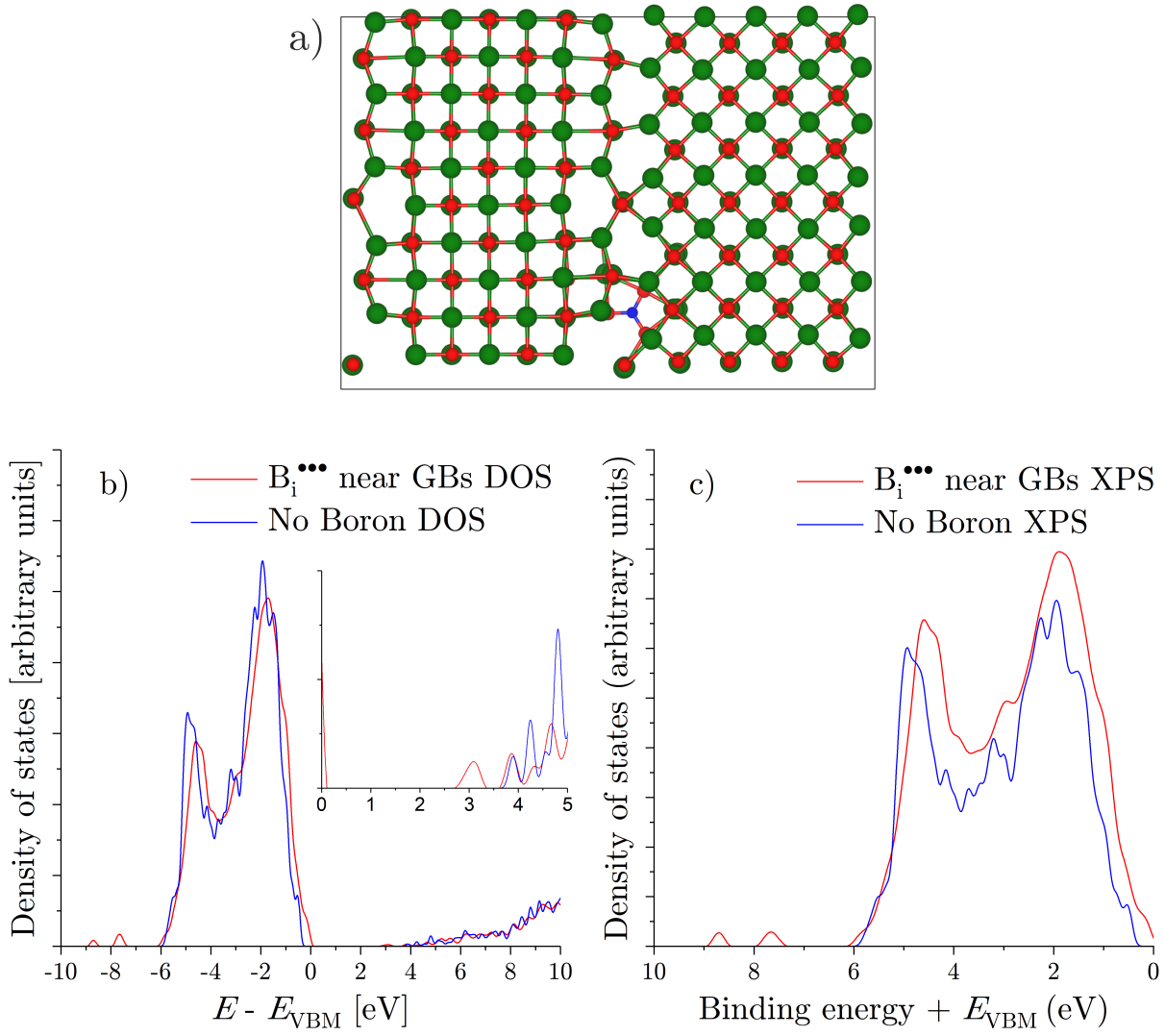

FIG. 6. Figure showing the difference in density of states between single boron interstitial at the grain boundary and no boron interstitial at the grain boundary for the asymmetric tilt grain boundary MgO supercell. a) A boron interstitial at the grain boundary of an MgO (100)/(110)[001] asymmetric tilt grain boundary b) Projected density of states using a hybrid functional (HSE06) for both supercells. Only atoms within 2.5 Å of the grain boundary are selected for the projected density of states. c) Simulated x-ray photoelectron spectroscopy spectrum for systems a). An inset in b) is shown to highlight the effect of B on the states in the band gap.

IV. DISCUSSION

The large variation in the electrostatic potential near the ATGB and STGB studied in this paper suggests the possibility of other defects being favoured at grain boundaries over the bulk including

positively charged point defects. Although beyond the scope of this work positively charged point defects in MgO may make for interesting further study.

Just before submission of this manuscript a STEM-EELS and transport investigation of B diffusion in MgO MTJs was published that provides clear evidence for the presence of B at MgO GBs[38]. In the experimental work the difference in boron diffusion between two different underlayers is shown. The experimental study revealed that significantly more boron diffusion occurred into the grain boundaries of MgO with a W underlayer over a Ta underlayer. The experimental study used STEM and EELS to atomistically resolve the structures and chemical detail within the MgO layer. There is still opportunity for a study involving XPS to measure the electronic effects of boron within the MgO layer. The paper proposed boron to be in a trigonal coordination ($[BO3]^{-3}$ configuration) which is identical what is found computationally. The increase in boron within the MgO layer gave rise to a reduction of the resistance-area product due to enhanced GB transport but the magneto-resistance was similar. These results are in very good agreement with our predictions and the fact these studies were performed completely independently adds further weight to the conclusions.

V. CONCLUSIONS

In this paper point defects near MgO GBs have been investigated. It has been found that oxygen vacancies are more energetically favourable the closer they are to the grain boundaries of either the STGB or ATGB. Further it is found that the segregation energy of the oxygen vacancies in the ATGB can be as high as 1.8 eV while for the STGB the segregation energy is around 0.6 eV. The results are significant as these GBs are observed experimentally in MTJs and so may be oxygen poor at GBs which may in turn be further reducing the theoretically determined TMR in these devices[11,15]. It can be concluded that oxygen vacancies are likely to form near GBs in MgO thin films.

The segregation energy of the $B_i^{\bullet\bullet\bullet}$ point defect is considerably larger than oxygen vacancies, 4.2 eV in the STGB and 4.5 eV in the ATGB. The high segregation energy of boron interstitials in GBs is due to the large relative instability difference as boron is energetically unfavourable in the bulk of MgO. It was not found that $B_O^{\times}$ point defects were stable in either the STGB or ATGB systems. Further to determining the segregation energy first principles calculations have been employed to determine the PDOS of boron within the GBs. In the PDOS boron appears as

two additional peaks in the DOS spectrum below the valence band. It may be possible to detect the boron peaks using experiments such as XPS or UPS. Such an experiment would add to the growing body of evidence that boron can exist within the MgO layer of MTJs and hence be affecting the electronic transport properties.

ACKNOWLEDGMENTS

We would like to acknowledge financial support from the EPSRC (EP/K003151) and facilities support from the N8 Consortium (Polaris supercomputer), Materials Chemistry Consortium (Archer supercomputer, EPSRC grant EP/L000202). We would also like to acknowledge that some of this work was performed using resources provided by the Cambridge Service for Data Driven Discovery (CSD3) operated by the University of Cambridge Research Computing Service (http://www.csd3.cam.ac.uk/), provided by Dell EMC and Intel using Tier-2 funding from the Engineering and Physical Sciences Research Council (capital grant EP/P020259/1), and DiRAC funding from the Science and Technology Facilities Council (www.dirac.ac.uk). All data relating to the theoretical calculations created during this research are available by request from the University of York Research database http://dx.doi.org/yyy. We give special thanks to Prof A. Lindsay Greer and Dr Nikolaos Panagiotopoulos for useful conversations about experiments including XPS.

---

* jb2191@cam.ac.uk

† keith.mckenna@york.ac.uk

[1] S. Tehrani, J. M. Slaughter, E. Chen, M. Durlam, J. Shi, and M. Deherrera, IEEE Transactions on Magnetics **35**, 2814 (1999).

[2] X. Dong, X. Wu, G. Sun, Y. Xie, H. Li, and Y. Chen, Proceedings - Design Automation Conference , 554 (2008).

[3] S. Bader and S. Parkin, Annual Review of Condensed Matter Physics **1**, 71 (2010).

[4] K. C. Chun, H. Zhao, J. D. Harms, T. H. Kim, J. P. Wang, and C. H. Kim, IEEE Journal of Solid-State Circuits **48**, 598 (2013).

[5] S. Fujita, H. Noguchi, K. Nomura, K. Abe, E. Kitagawa, N. Shimomura, and J. Ito, IEEE Transactions on Magnetics **49**, 4456 (2013).

[6] E. Y. Tsymbal, O. N. Mryasov, and P. R. LeClair, Journal of Physics: Condensed Matter **15**, R109 (2003).

[7] J.-G. J. Zhu and C. Park, Materials Today **9**, 36 (2006).

[8] S. Ikeda, J. Hayakawa, Y. Ashizawa, Y. M. Lee, K. Miura, H. Hasegawa, M. Tsunoda, F. Matsukura, and H. Ohno, Applied Physics Letters **93**, 39 (2008).

[9] W. H. Butler, Science and Technology of Advanced Materials **9**, 014106 (2008).

[10] J. Mathon and A. Umerski, Physical Review B **63**, 220403 (2001).

[11] W. H. Butler, X.-G. Zhang, T. C. Schulthess, and J. M. MacLaren, Physical Review B **63**, 054416 (2001).

[12] X. G. Zhang and W. H. Butler, Physical Review B **70**, 1 (2004), 0409155.

[13] S. Yuasa, T. Nagahama, A. Fukushima, Y. Suzuki, and K. Ando, Nature Materials **3**, 868 (2004).

[14] S. S. P. Parkin, C. Kaiser, A. Panchula, P. M. Rice, B. Hughes, M. Samant, and S.-H. Yang, Nature Materials **3**, 862 (2004).

[15] J. J. Bean, M. Saito, S. Fukami, H. Sato, S. Ikeda, H. Ohno, Y. Ikuhara, and K. P. McKenna, Scientific Reports **7**, 45594 (2017).

[16] S. G. Wang, G. Han, G. H. Yu, Y. Jiang, C. Wang, A. Kohn, and R. C. C. Ward, Journal of Magnetism and Magnetic Materials **310**, 1935 (2007).

[17] D. Harris, G. Watson, and S. Parker, Physical Review B **56**, 11477 (1997).

[18] B. P. Uberuaga, X.-M. Bai, P. P. Dholabhai, N. Moore, and D. M. Duffy, Journal of Physics: Condensed Matter **25**, 355001 (2013).

[19] K. P. McKenna and A. L. Shluger, Physical Review B **79**, 1 (2009).

[20] Z. Wang, M. Saito, K. P. McKenna, S. Fukami, H. Sato, S. Ikeda, H. Ohno, and Y. Ikuhara, Nano Letters **16**, 1530 (2016).

[21] K. Tsunekawa, Y. S. Choi, Y. Nagamine, D. D. Djayaprawira, T. Takeuchi, and Y. Kitamoto, Japanese Journal of Applied Physics, Part 2: Letters **45**, (2006).

[22] V. Harnchana, A. T. Hindmarch, M. C. Sarahan, C. H. Marrows, A. P. Brown, and R. M. D. Brydson, Journal of Applied Physics **113**, (2013).

[23] Y. Lu, B. Lépine, G. Jézéquel, S. Ababou, M. Alnot, J. Lambert, A. Renard, M. Mullet, C. Deranlot, H. Jaffrès, F. Petroff, and J. M. George, Journal of Applied Physics **108**, (2010).

[24] F. Guo, Z. Wu, T. Chen, Y. Wu, G. Cai, and J. Kang, Computational Materials Science **101**, 138 (2015).

[25] I. A. Pašti and N. V. Skorodumova, Phys. Chem. Chem. Phys. **18**, 426 (2016).

[26] H. K. Chandra and P. Mahadevan, Physical Review B **89**, 1 (2014).

[27] J. Heyd, G. E. Scuseria, and M. Ernzerhof, Journal of Chemical Physics **118**, 8207 (2003).

[28] N. A. Benedek, A. L. S. Chua, C. Elsässer, A. P. Sutton, and M. W. Finnis, Physical Review B **78**, 1 (2008).

[29] J. J. Bean and K. P. McKenna, Acta Materialia **110**, 246 (2016).

[30] P. Hohenberg and W. Kohn, Physical Review **136**, B864 (1964).

[31] W. Kohn and L. J. Sham, Physical Review **140**, (1965).

[32] G. Kresse and J. Hafner, Physical Review B **47**, 558 (1993).

[33] G. Kresse and J. Hafner, Physical Review B **49**, 14251 (1994).

[34] J. P. Perdew, K. Burke, and M. Ernzerhof, Physical Review Letters **77**, 3865 (1996).

[35] J. J. Bean and K. P. McKenna, 1 **Supplementary Material, PRM, 1**, 1 (1).

[36] A. J Jackson, A. M Ganose, A. Regoutz, R. G. Egdell, and D. O Scanlon, Journal of Open Source Software **3**, 773 (2018).

[37] U. Gelius and K. Siegbahn, General Discussions of Faraday Society **54**, 257 (1972).

[38] X. Xu, K. Mukaiyama, S. Kasai, T. Ohkubo, and K. Hono, Acta Materialia **161**, 360 (2018).